

Phase mixing and phase motion of Alfvén waves on tail-like and dipole-like magnetic field lines

Andrew N. Wright

Mathematical Institute, University of St. Andrews, Fife, Scotland

W. Allan

National Institute of Water and Atmospheric Research, Wellington, New Zealand

R. D. Elphinstone and L. L. Cogger

Department of Physics and Astronomy, University of Calgary, Calgary, Canada

Abstract. The time-dependent phase structure of Alfvén waves on open and closed field lines is studied. In accord with previous observations we find that Alfvén waves on near-Earth closed field lines exhibit a poleward phase motion unless they are close to the plasmopause, in which case the motion may be equatorward. Alfvén waves generated on tail-like closed or open field lines threading the plasma sheet boundary layer have received much less attention but may be shown to have an equatorward phase motion [*Liu et al.*, 1995]. Phase mixing in the magnetotail proves to have a much richer behavior than that on near-Earth (dipole-like) closed field lines as not only the Alfvén frequency varies across the background field lines but the field-aligned wavenumber varies too. The two contributions tend to cancel each other partially for typical tail equilibria. Observations are given of a double oval configuration showing long-period pulsations on the poleward portion of this oval. Equatorward phase motion is observed and supports the theory presented here. These observations illustrate that Pc5 pulsation activity can be much richer than previously thought and can occur at locations not in the dipole-like region, as is usually supposed. The concepts presented in this paper provide a powerful framework with which to interpret observations related to auroral arcs, substorms, and magnetospheric equilibria.

1. Introduction

Observations of ultra-low-frequency (ULF) waves provide a rich source of information about the system in which they exist. On the simplest level, the frequency of the wave is of the order of the ratio of the typical propagation speed to the size of the system. The fact that waves are observed at all indicates there is coupling to an energy source and details of the source and coupling mechanisms may be gleaned from careful examination of observations.

Once waves have been established, the manner in which they propagate and disperse can be related to properties of the medium which carries the wave. In the past, observations of Alfvén wave polarization by *Samson et al.* [1971] and the theoretical treatment of *Southwood* [1974] were crucial in establishing the “field line resonance” concept that has been so successful in

understanding small- m toroidal pulsations, where m is the dimensionless azimuthal wavenumber.

It is not surprising that Alfvén waves were at the heart of early studies by *Samson et al.* [1971] and *Southwood* [1974]: Alfvén waves are very robust waves, and their field-guided propagation means they maintain their amplitude and are long-lived. They also have a strong magnetic signature on the ground [*Hughes*, 1974] and so are relatively easy to observe.

Satellite observations of ULF waves have an ambiguity between spatial and temporal variations. The advances discussed above have come from ground-based observations of the magnetic fields associated with ULF waves which are able to resolve their behavior in space and time. Indeed, ground-based observations of the ionospheric foot points of ULF waves provide the most promising methods of studying the waves’ detailed structure. For example, radar observations [*Walker et al.*, 1979] have provided compelling evidence supporting the field line resonance (FLR) model of *Southwood* [1974].

More recently, *Samson et al.* [1991] have studied meridian scanning photometer data and found the same

Copyright 1999 by the American Geophysical Union.

Paper number 1999JA900018.
0148-0227/99/1999JA900018\$09.00

frequencies present in simultaneous radar and optical observations. This study suggests that FLRs can modulate the optical auroral emissions. The coincidence of spectral peaks in simultaneous magnetometer and radar data was reported by *Samson et al.* [1992], who also found the classic field line resonance signature: a phase change of π across the amplitude maximum in both data sets. *Xu et al.* [1993] confirmed that FLRs could directly modulate auroral emissions by studying magnetometer and photometer data. Not only did the two data sets have common spectral peaks, but the optical data were found to have classic π phase change.

The mechanisms through which ULF waves accelerate the particles that produce auroral emissions are still a matter of debate. *Wei et al.* [1994] suggest that the ULF waves phase mix down to scales of order the electron inertial length, at which point parallel electric fields are generated that may accelerate particles. *Wright and Allan* [1996a] note that ionospheric dissipation causes the waves to die out before they are able to phase mix to this extent. If ULF waves do produce scales of order the electron inertial length it is not clear how they do so within linear theory. (Of course, these scales may already exist in the equilibrium supporting the waves or be produced by nonlinear effects.)

Most studies of Alfvén waves have focused upon how they are established on closed field lines and the properties of such waves (see the reviews by *Allan and Poulter* [1992], *Hughes* [1994], and *Wright* [1994a]). Recently, the question of establishing Alfvén waves on very tail-like or open magnetotail field lines has been addressed, and most of the present paper concentrates on the phase properties of these waves. *Liu et al.* [1995] considered ULF waves on closed (dipole-like) field lines in addition to open (tail-like) field lines. The latter problem had also been addressed by *Goertz and Smith* [1989] and *Seboldt* [1990]. *Liu et al.* [1995] considered a one-dimensional wave model (solving across the current sheet, plasma sheet boundary layer (PSBL), and lobe), and also analyzed high-latitude optical data. Both theory and data produced equatorward arc motion for field lines threading the PSBL. This is in contrast to what is generally observed on closed field lines and is a very useful diagnostic. The modeling of ULF waves in the tail has been refined recently by *Allan and Wright* [1998], who extended the analysis to two dimensions. This enabled them to model realistically the way in which ULF waves propagate along the tail and couple to one another. Their solutions provide a much richer wave structure than earlier models, and we exploit this when analyzing and interpreting some optical auroral data.

Our analysis indicates an equatorward phase motion for field lines mapping to the PSBL, and excellent agreement is found with optical data from the poleward auroral oval whose field lines map to the PSBL [e.g., *Elphinstone et al.*, 1995b].

The paper is structured as follows: Section 2 addresses phase mixing of Alfvén waves on closed field lines. Section 3 considers the phase properties of Alfvén

waves excited on open field lines mapping to the PSBL. Section 4 presents observations of optical emissions from nightside auroral arcs, and section 5 compares these observations with the model of section 3. Section 6 summarizes our results.

2. Phase Mixing on Closed Dipole-like Field Lines

Auroral radar observations of the foot points of closed field lines supporting standing Alfvén waves [e.g., *Kaneda et al.*, 1964; *Keys*, 1965; *Brooks*, 1967] reveal sloping patches in range-time-intensity (RTI) plots. These observations revealed a clear poleward motion at mid-to-high latitudes. The steady state theory of field line resonances [*Tamao*, 1965; *Southwood*, 1974] has been shown to fit very well with Scandinavian Twin Auroral Radar Experiment (STARE) observations [*Walker et al.*, 1979]. In particular, there is a phase change of π across the pulsation and poleward phase motion when the Alfvén frequency ($\omega_A(L)$) decreases with L (the McIlwain parameter). This periodically repeating poleward motion has also been seen in optical auroral data [*Elphinstone and Hearn*, 1993; *Xu et al.*, 1993] and is directly related to the poleward moving structures seen in the radar data [*Nielsen et al.*, 1993].

A steady state pulsation may be thought of as the large time limit of a time-dependent pulsation, and below we examine the phase motion from a time-dependent perspective. Figure 1 shows the Earth and two closed field lines labeled L_1 and L_2 . For typical mid-to-high latitude field lines, ω_A decreases between L_1 and L_2 so that

$$\frac{d\omega_A(L)}{dL} < 0 \quad (1)$$

The situation may be quite different near the plasma-pause where $d\omega_A(L)/dL > 0$ due to mass loading of plasmaspheric sections of the field lines, and we return to this point later. *Mann et al.* [1995] showed that even though the Alfvén waves are coupled to the fast mode, the phase of the Alfvén waves evolves in an essentially decoupled or free oscillation. Toroidal Alfvén

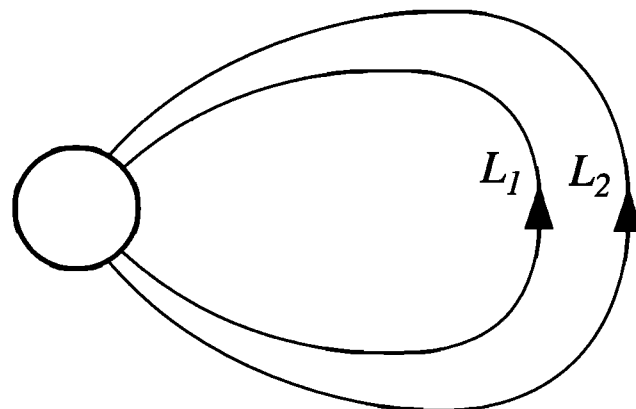


Figure 1. A schematic view of two closed field lines (labeled L_1 and L_2) and Earth.

waves consisting of predominantly one harmonic have the solution

$$b_\phi \approx A(L, \lambda) \exp i[-\omega_A(L)t] \quad (2)$$

where $\omega_A > 0$. $A(L, \lambda)$ gives the structure of the mode along the field line (in terms of the latitude λ) and the amplitude variation across L shells. Of course, (2) does not represent the full solution to the coupled equations. In particular, it does not get the time variation of the amplitude A correct. However, the present study is only concerned with the phase of the waves, and the form given in (2) determines this well; see, for example, Figure 9 of *Rickard and Wright* [1994].

Assuming that A is real, or a slowly varying function of L , we can write the phase of the wave in (2) as

$$\phi = -\omega_A(L)t \quad (3)$$

If we now follow a point of constant phase (setting $\phi = \text{const}$), equation (3) gives the trajectory $L(t)$ for the chosen phase. Taking the time derivative of (3) yields $(d\omega_A/dL)(dL/dt)t + \omega_A = 0$. The phase velocity across L shells is simply

$$V_{pL} = \frac{dL}{dt} = \frac{-\omega_A}{(d\omega_A/dL)t} \quad (4)$$

To calculate the phase velocity in ms^{-1} at some position along the field line (e.g., the equatorial plane or the ionosphere), we need to know the distance (w) that a unit L interval maps to (w will vary along the field line). The phase velocity is then $w dL/dt \text{ ms}^{-1}$ and is easily calculated from (4).

Previously, the phase of the waves has been studied in terms of the phase mixing length (L_{ph}), and it is easy to show that this yields the same phase velocity as (4). Consider a snapshot of the Alfvén waves described in (2). The oscillatory nature of the solution across L shells could be described by a slowly varying local wavenumber $k_L(L)$ such that $b_\phi \propto \exp i(k_L L)$. Therefore

$$ik_L \approx \frac{1}{b_\phi} \frac{\partial b_\phi}{\partial L} \equiv \frac{1}{A} \frac{\partial A}{\partial L} - i \frac{d\omega_A}{dL} t \quad (5)$$

the final relation above employing the solution (2). If A is a slowly varying function of L , or we wait for a suitably long time, the second term on the right-hand side of (5) will dominate over the first, yielding $k_L \approx -(d\omega_A/dL)t$. The phase mixing length is just the local wavelength in the L direction

$$L_{ph} = \frac{2\pi w}{(d\omega_A/dL)t} \quad (6)$$

and demonstrates that as time increases, the adjacent field lines drift out of phase more and generate smaller spatial scales. The phase velocity of the phase mixing is simply $V_{pL} = \omega_A(L)/k_L$, which provides an alternative route to the result in (4).

For the closed field lines satisfying (1) we make a clear prediction from (4) that the phase velocity should be in the direction of increasing L , i.e., poleward for ionospheric observations. This is in agreement with the observations discussed earlier. We noted previously that near the plasmopause, $d\omega_A/dL$ may have the opposite sign to that in (1). It is evident from (4) that the sense of the phase velocity will switch in this case too, and the phase motion will be equatorward. (Note that this is still in the direction of the local decrease in ω_A .) Indeed, observations of such “reversed” phase motion are also well documented [e.g., *Nielsen and Allan*, 1983].

According to (4) the phase velocity should be very large at early times and decrease as $1/t$. In RTI plots this would correspond to arcs having a positive gradient that decreases in time. This decrease of slope in time is exactly what is observed in the case of the short-lived events known as “transient” pulsations [e.g., *Poulter et al.*, 1984]. The decrease in phase speed can also be seen very clearly in Figure 3 of *Samson et al.* [1996]. These have been interpreted as impulsively excited freely ringing dipole-like magnetic field shells. On some occasions, very large poleward phase speeds at early times have been observed. However, for an event driven quasi-monochromatically over a finite time, the waves may be too small to be observed at early times when V_{pL} is changing most rapidly. When ionospheric damping is taken into account, there is a lower limiting phase speed which implies a smallest scale that the waves can phase mix down to. *Mann et al.* [1995] and *Allan and Wright* [1997] showed that if a single Alfvén wave decays at a rate γ , the limiting phase mixing length is

$$L_{AS} = \frac{\pi w \gamma}{(d\omega_A/dL)} \quad (7)$$

which agrees with the width of a steadily driven resonance to within a factor of $\pi/4$ (see δ_B of *Wright and Allan* [1996b]). Thus there is a corresponding lower limit on the phase speed of $V_{pL} = -\gamma \omega_A w / (2d\omega_A/dL)$. Although this behavior has not been demonstrated unequivocally in observed events, it is quite clear in the numerically simulated RTI plots in Figure 3 of *McDermid and Allan* [1990].

For times larger than $2/\gamma$ the steady state modes may be employed, but for earlier times the above time-dependent treatment is appropriate. It is encouraging that the principal feature of the steady state model, namely, the poleward phase motion, is still found in our time-dependent calculation. This property may be seen very clearly in Figure 2 of *Fenrich et al.* [1995], in which the RTI plot shows arcs with a positive slope for closed field lines mapping to the dawn flank.

3. Phase Mixing on Tail-like Field Lines

A model magnetotail containing stretched tail-like field lines is shown in Figure 2. The x origin has been shifted deep into the tail to coincide with the source region of fast mode waves (e.g., a plasmoid ejection) that

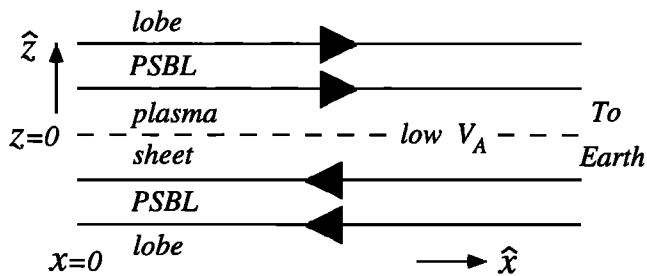


Figure 2. An idealized model of the magnetotail. The x origin has been shifted to coincide with the source of waves deep in the tail.

perturbs the system. Field lines in the $x < 0$ region are very tail-like, while those in the $x > 0$ region will gradually become more dipole-like as Earth is approached. The tail-like field line region shall be treated as an open field line region since the waves we consider only realize that the field lines are closed after the round-trip travel time, and we are interested in times shorter than this. The Alfvén speed is smallest in the plasma sheet ($z = 0$) and increases monotonically through the PSBL and into the tail lobes. The equilibrium is one-dimensional.

The equilibrium in Figure 2 (except for the reversal in field direction across $z = 0$) is very similar to simple models of open solar field lines in the corona. Indeed, phase mixing of Alfvén waves has been proposed as a method of heating the corona and several theoretical studies completed [e.g., Ireland and Priest, 1997; Hood *et al.*, 1997, and references therein]. Solar studies do not generally address the mechanism through which the Alfvén waves are excited, other than to assume a steady monochromatic driver. The normal modes of these studies have a single frequency of oscillation that is common to each field line, in contrast to the closed field line situation of section 2. In the latter case the field-aligned wavenumber ($\equiv \omega/V_A(z)$) is different for each field line and produces phase mixing in space rather than time.

The coupling of waves in a model equilibrium such as that in Figure 2 has been considered previously by Goertz and Smith [1989], Seboldt [1990], and Liu *et al.* [1995]. All these models focused upon normal modes with a single wavenumber along the tail and were thus unable to address the manner in which waves propagate and disperse as they travel along the tail. (The wave solutions are one-dimensional.) Goertz and Smith [1989] considered the energy source to be waves propagating in from the magnetopause, whereas Liu *et al.* [1995] considered a source in the plasma sheet associated with a substorm. We favor the latter source in our model.

Allan and Wright [1998] extended the modeling of waves in the tail to two-dimensional solutions and focused upon the details of propagation along the tail. They showed how a general source of fast modes could couple to Alfvén waves for a system like that in Figure

2. The key to understanding the coupling process is the fast and Alfvén dispersion diagrams. For the variation of Alfvén speed described earlier, fast modes tend to be trapped in the middle of the tail “waveguide.” For a given k_y and harmonic number in z , Figure 3a shows how the fast frequency varies with field-aligned wavenumber. Figure 3b displays the dependence of the field-aligned group velocity ($V_{g\parallel} = \partial\omega/\partial k_{\parallel}$) on k_{\parallel} and the asymptote for large k_{\parallel} ; $V_{g\parallel} \rightarrow V_A(z = 0)$, see Wright [1994b].

Allan and Wright [1998] demonstrated how to determine the frequency ($\omega_A(z)$) and field-aligned wavenumber ($k_{\parallel A}(z)$) of the resonantly excited Alfvén waves on the field line at a given z . These waves are driven by the

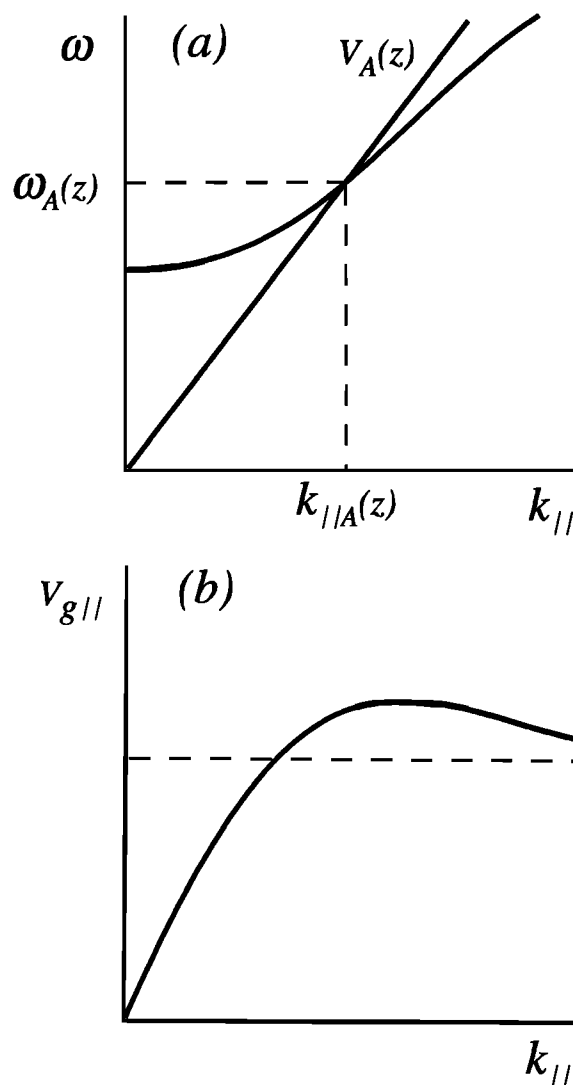


Figure 3. (a) The generic dispersion diagram and (b) field-aligned group velocity for the fast mode in a typical tail equilibrium (k_y has a fixed value). On a field line at given z in Figure 3a the intersection of $\omega = k_{\parallel} V_A(z)$ with the fast curve identifies $\omega_A(z)$ and $k_{\parallel A}(z)$, the frequency and wavenumber of the Alfvén wave that is resonantly excited at z . The dashed line in Figure 3b shows the asymptotic value of $V_{g\parallel}$ for large k_{\parallel} .

fast mode wave components that have the same field-aligned phase speed as the Alfvén waves, i.e., $V_A(z)$. The line with slope $V_A(z)$ is indicated in Figure 3a, and where it crosses the fast mode dispersion curve the values of $\omega_A(z)$ and $k_{\parallel A}(z)$ are defined. Of course, if more than one fast harmonic across the tail is excited, it will be necessary to include other fast dispersion curves in Figure 3, and this raises the possibility that Alfvén waves with several values of ω_A and $k_{\parallel A}$ may be excited on a single field line. In section 3.1 we shall assume that only one fast harmonic (in z) is responsible for driving Alfvén waves, and this condition will be relaxed in section 3.2.

3.1. Single Fast Harmonic Mode Excitation

For simplicity, the Alfvén response driven by a single fast waveguide mode harmonic is considered. By this we mean a single harmonic standing across the tail (in z), but consider all field-aligned wavenumbers (k_y is fixed). This situation was used to explain the results of *Allan and Wright* [1998]. These are summarized in Figure 4, which is a snapshot of the wave fields. Figure 4a shows how Alfvén waves in an elemental layer dz around the resonance position z_r are driven by the fast mode components in the interval dk_{\parallel} around $k_{\parallel A}(z)$. These fast modes propagate along the guide at a speed $V_{g\parallel}(k_{\parallel A}(z_r))$ (which we write in shorthand as $V_{g\parallel}(z_r)$ from now on). Since the waves were initiated at $x = t = 0$, fast modes that couple resonantly to Alfvén

waves at z_r will only have propagated a distance x_f along the tail, whereas Alfvén waves will have traveled a distance x_A , where

$$x_f = V_{g\parallel}(z_r)t, \quad x_A = V_A(z_r)t \quad (8)$$

Thus the section of field line (at z_r) satisfying $x_f(z_r) < x < x_A(z_r)$ is filled with Alfvén waves radiated from the propagating fast mode. No information has reached the region $x > x_A(z_r)$, and the section $0 < x < x_f(z_r)$ is perturbed by fast modes with $k_{\parallel} < k_{\parallel A}(z_r)$. When considering other field lines (with different V_A), ω_A and $k_{\parallel A}$ will change, as will the points separating fast/Alfvén/unperturbed regions. Figure 4b gives the qualitative features of the distribution of different waves across the entire width of the tail. Note that the boundaries $x_A(z)$ and $x_f(z)$ separate the domains of resonant waves, which are likely to dominate the observable signatures. Nonresonant waves will not obey the strict demarcation of Figure 4 but were of much smaller amplitude in the simulations of *Allan and Wright* [1998].

When studying the phase mixing of Alfvén waves, it is important to determine how ω_A and $k_{\parallel A}$ change with z . On each field line we must satisfy the Alfvén wave dispersion relation

$$\omega_A(z) = k_{\parallel A}(z)V_A(z) \quad (9)$$

Suppose we move to a neighboring field line with different V_A . This means the slope of the straight line in

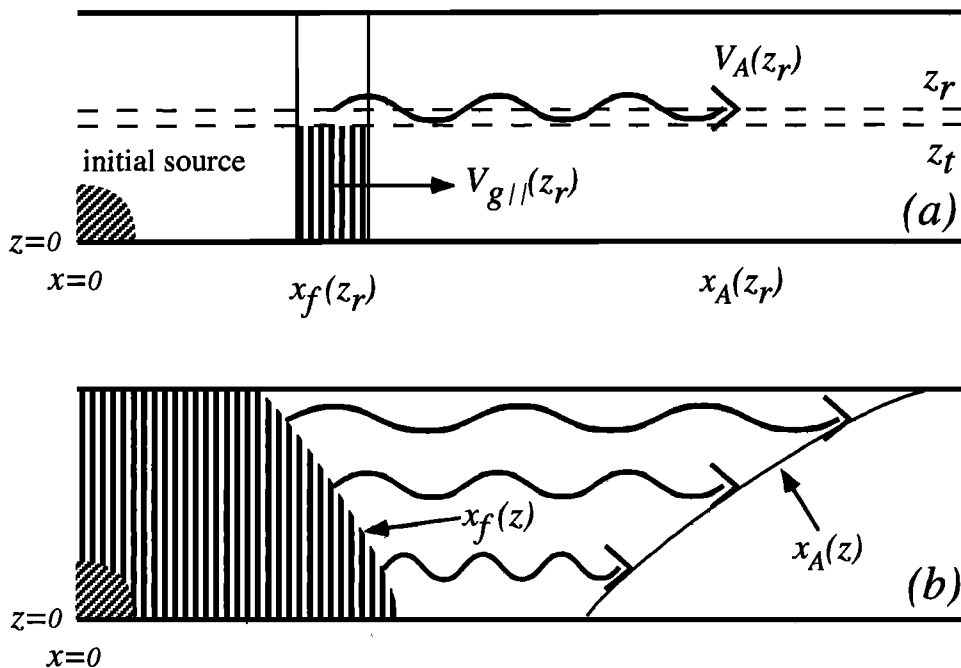


Figure 4. (a) A snapshot of the fast mode components in the interval $k_{\parallel} \rightarrow k_{\parallel} + dk_{\parallel}$ that have a turning point at z_t . (Only the northern tail is shown.) These waves couple to an Alfvén wave at $z_r \approx z_t$ (for small k_y) that is radiated ahead of the fast mode if $V_A(z) > V_{g\parallel}(k_{\parallel} = k_{\parallel A}(z_r))$, which is generally the case. (b) A snapshot of the distribution of fast and Alfvén waves for all k_{\parallel} components and z values.

Figure 3a will change; consequently, the point of the intersection of the curves changes, and our solution has a new ω_A and $k_{\parallel A}$. However, the changes $d\omega_A$ and $dk_{\parallel A}$ are constrained so that the solution lies on the fast dispersion curve. Therefore

$$\frac{d\omega_A}{dk_{\parallel A}} = V_{g\parallel}(k_{\parallel A}) \quad (10)$$

Differentiating (9) with respect to z gives

$$\frac{d\omega_A}{dz} = \frac{dk_{\parallel A}}{dz} V_A + k_{\parallel A} \frac{dV_A}{dz} \quad (11)$$

Employing the chain rule

$$\frac{d\omega_A}{dz} = \frac{d\omega_A}{dk_{\parallel A}} \frac{dk_{\parallel A}}{dz} \equiv V_{g\parallel}(k_{\parallel A}) \frac{dk_{\parallel A}}{dz} \quad (12)$$

equation (11) may be rewritten as either

$$\frac{d\omega_A}{dz} = -\frac{dV_A}{dz} k_{\parallel A} \frac{V_{g\parallel}}{V_A - V_{g\parallel}} \quad (13)$$

or

$$\frac{dk_{\parallel A}}{dz} = -\frac{dV_A}{dz} k_{\parallel A} \frac{1}{V_A - V_{g\parallel}} \quad (14)$$

(Note these relations are solely functions of z since $V_{g\parallel} \equiv V_{g\parallel}(k_{\parallel} = k_{\parallel A}(z))$, which we write as $V_{g\parallel}(z)$ for brevity.)

Allan and Wright [1998] showed how the phase of the Alfvén waves in the region $x_f < x < x_A$ could be represented accurately in the form $\exp i\phi$,

$$\phi = k_{\parallel A}(z)x - \omega_A(z)t \quad (15)$$

Differentiating with respect to z gives the local wavenumber in z ,

$$k_z(z) = \frac{\partial \phi}{\partial z} = \frac{dk_{\parallel A}}{dz}(x - V_{g\parallel}t) \quad (16)$$

where we have used the relation in (12). The phase mixing length in z ($L_{ph} = |2\pi/k_z|$) and the phase velocity in z ($V_{pz} = \omega_A(z)/k_z$) may be determined using (14) and (16)

$$L_{ph} = \frac{2\pi}{k_{\parallel A}(dV_A/dz)} \cdot \frac{V_A - V_{g\parallel}}{x - V_{g\parallel}t} \quad (17)$$

$$V_{pz} = \frac{-V_A}{dV_A/dz} \cdot \frac{V_A - V_{g\parallel}}{x - V_{g\parallel}t} \quad (18)$$

Figure 4 was constructed under the assumption that $V_A(z) > V_{g\parallel}(z)$, which will be true if the dispersion curves in Figure 3 only have one point of intersection. If the curves intersected twice, one root would have $V_{g\parallel}(z) > V_A(z)$. In this case, the fast mode would propagate more quickly than the Alfvén wave which would no longer be radiated ahead of the fast mode but would be left in its wake. When $V_{g\parallel} > V_A$, Figure 4 needs to be modified. However, we believe that typical magneto-

tail equilibria will have $V_A(z) > V_{g\parallel}(z)$, and so we will focus on this ordering for the remainder of the present paper.

Alfvén waves only exist in the region $x > x_f(z)$ when $V_A(z) > V_{g\parallel}(z)$, so equation (18) indicates that the phase velocity in z is opposite to ∇V_A . Points of constant phase move from high Alfvén speed to low Alfvén speed field lines. For the model in Figure 2, the motion will be equatorward when the field lines are mapped to the ionosphere.

It is interesting to note that phase mixing now has contributions from both ω_A and $k_{\parallel A}$ varying across \mathbf{B} , unlike previous studies that focused upon one or other of these terms. Moreover, $dk_{\parallel A}/dz$ contributes the term involving x in (16), whereas $d\omega_A/dz$ contributes the $V_{g\parallel}t$ term. Evidently, these two terms are of opposite sign and tend to cancel each other partially. Since $x > V_{g\parallel}t$, it is the $k_{\parallel A}$ phase mixing that dominates and determines the direction of the phase motion.

On a given field line, the maximum phase mixing occurs in the leading edge of the Alfvén wave ($x = x_A(z) = V_A(z)t$), and it is here that the minimum phase mixing length and phase velocity are found:

$$\min L_{ph} = \frac{2\pi}{k_{\parallel A}(dV_A/dz)t} \quad (19)$$

$$\min V_{pz} = \frac{-V_A}{(dV_A/dz)t} \quad (20)$$

Moving back from the Alfvén wave leading edge x_A toward the fast mode leading edge x_f , the phase mixing length and phase speed both increase, becoming infinite at x_f , indicating that Alfvén waves are radiated with a locally coherent phase in z .

Besides studying the phase properties of a snapshot like that in Figure 4, it is useful to consider these properties as a function of time at a fixed distance x_0 away from the source. This is particularly useful for interpreting satellite or ionospheric observations. For observations centered upon the field line z_0 , nothing is seen during $0 < t < x_0/V_A(z_0)$. At $t = x_0/V_A(z_0)$ the first Alfvén waves arrive with phase properties given in (19) and (20). Over the interval $x_0/V_A(z_0) < t < x_0/V_{g\parallel}(z_0)$, Alfvén waves continue to arrive and L_{ph} and V_{pz} increase with t . No Alfvén waves are observed for $t > x_0/V_{g\parallel}(z_0)$, although fast waves may be present. These ideas indicate that the phase speed observed in the ionosphere will increase with time for Alfvén waves on tail-like field lines. This is exactly the opposite behavior to that expected on dipole-like field lines (see section 2) and could provide a useful diagnostic.

3.2. Multiple Fast Harmonic Mode Excitation

We next generalize the above analysis to consider the Alfvén waves that will result when more than one fast mode harmonic (in z) is present. Of course, a continuum of k_{\parallel} is still permitted. In the linear limit we can consider each fast harmonic independently and con-

struct a diagram like Figure 4b for each one. The total wave field generated by many fast harmonics is then the sum of these diagrams.

Suppose our initial condition contains several fast harmonics. These could be represented by including additional dispersion curves on Figure 3a, $\omega_n(k_{\parallel})$, which may have intersections with the straight line $V_A(z)$ at $(\omega_{An}, k_{\parallel An})$, where $n=1,2,3,\dots$. The field line at z , with Alfvén speed $V_A(z)$, will have several Alfvén waves resonantly excited on it with frequencies and wavenumbers given by these intersection values. Assuming that the initial source of all fast harmonic is the same point ($x = 0$), then all the leading edges, $x_A(z)$, will coincide. However, the trailing edges, $x_f(z)$, will not coincide as the group velocity of each fast harmonic, $V_{g\parallel n}(k_{\parallel An})$, will vary with n . We write these group velocities as simply $V_{g\parallel n}(z)$, since $k_{\parallel An}$ is solely a function of z .

For an ensemble of fast harmonics initiated at $x = t = 0$, consider the waves seen at x_0 (e.g., the ionosphere) on the field line at z . The Alfvén waves driven at z by all fast mode harmonics travel at $V_A(z)$, and so all arrive together at x_0 at a time $t_0 = x_0/V_A(z)$. The phase speed in z of each Alfvén wave component (V_{pzn}) as it arrives at x_0 may be calculated from (20), while the phase mixing length (L_{phn}) follows from (19),

$$V_{pzn}(x_0, z, t_0) = \frac{-V_A^2(z)}{x_0 dV_A/dz} \quad (21)$$

$$L_{phn}(x_0, z, t_0) = \frac{2\pi}{k_{\parallel An}(z)x_0 d \ln V_A/dz} \quad (22)$$

Note that although the initial phase mixing length varies with harmonic number n (through $k_{\parallel An}(z)$), the initial phase velocity is independent of n , suggesting a single slope should be seen in RTI plots initially. We now address how this phase velocity will evolve in time ($t > t_0$) using (18),

$$V_{pzn}(x_0, z, t) = \frac{-V_A}{dV_A/dz} \cdot \frac{V_A - V_{g\parallel n}}{x_0 - V_{g\parallel n}t} \quad (23)$$

Since we are only interested in times $t > t_0$ (where $t_0 = x_0/V_A(z)$), we introduce $t' = t - t_0$, and let $t' > 0$, to get

$$V_{pzn}(x_0, z, t' > 0) = \frac{-V_A^2}{x_0 dV_A/dz} \times \frac{1 - V_{g\parallel n}/V_A}{1 - V_{g\parallel n}/V_A - t'V_{g\parallel n}/x_0} \quad (24)$$

Note that when $t' = 0$, the above phase speed reduces to that in (21), as expected. For $t' > 0$ the phase speed will be a function of n through $V_{g\parallel n}$, although it may not show a strong dependence: In this paper we are assuming that $V_{g\parallel n}(z) < V_A(z)$. Indeed, for the magnetotail it is likely that $V_{g\parallel n}(z)/V_A(z) \ll 1$, in which case the phase velocity in (24) reduces to

$$V_{pzn}(x_0, z, t' > 0) = \frac{-V_A^2}{x_0 dV_A/dz} \cdot \frac{1}{1 - t'(V_{g\parallel n}/x_0)} \quad (25)$$

This indicates that when $V_{g\parallel n}(z)/V_A(z) \ll 1$, the phase speed (associated with the n th harmonic) changes on a timescale of $x_0/V_{g\parallel n}(z)$, which is equal to the time of flight of the fast mode. Signals arriving at x_0 for a duration t' much less than this timescale will show a fairly constant phase velocity in time. Moreover, the phase velocity will be independent of n . If different harmonic Alfvén waves are observed for a significant fraction of the fast mode time of flight, or if $V_{g\parallel n}(z)/V_A(z)$ is not much less than 1, they will evolve different phase speeds, and the unapproximated relation (24) must be employed.

3.3. Alfvén Wave Amplitudes

The analysis in this paper addresses the phase of Alfvén waves, but some remarks should be made about their amplitude. For example, *Allan and Wright* [1998] found that their driving condition only excited waves with $k_{\parallel} < k_{\parallel 0}$, where $k_{\parallel 0}$ is the wavenumber above which the driver power becomes negligible. Although the present calculation also describes waves for which $k_{\parallel} > k_{\parallel 0}$, these waves will have a small amplitude and be hard to observe in data and simulations. Another point to note is that for waves with $k_{\parallel} < k_{\parallel 0}$, which have a significant amplitude, the fast mode may decay as it couples to the Alfvén waves. This will result in the amplitude of the Alfvén waves decreasing as we move from x_A to x_f . Indeed, for very efficient coupling, only a few Alfvén cycles may be excited in the interval $x_A - \Delta x_d < x < x_A$, where $\Delta x_d \approx (V_A - V_{g\parallel})t_d$, and t_d is the decay time of the fast mode. The section $x_f < x < x_A - \Delta x_d$ may contain Alfvén waves of negligible amplitude.

It is interesting to note that once Alfvén waves begin to be reflected from the ionosphere, they will have the local structure of a standing Alfvén wave. In the linear theory presented here this will not affect the incident Alfvén wave. Inclusion of nonlinear effects will produce a ponderomotive force in the standing wave section that may be responsible for transporting ionospheric oxygen ions deep into the tail if the wave amplitude is large enough [*Allan*, 1993].

4. Auroral Observations

The fundamental conclusion of the section 3 is that Alfvén waves excited in regions of the magnetotail where $dV_A/dz > 0$ (especially in the PSBL) should exhibit an equatorward phase motion. This is in contrast to standing Alfvén waves on more dipole-like near-Earth closed field lines which generally have a poleward phase motion.

4.1. February 20, 1990, Event

Liu et al. [1995] have already presented observations of equatorward moving optical emissions, and we begin by looking at this data again. Plate 1 is a keogram plot (intensity as a function of latitude and universal

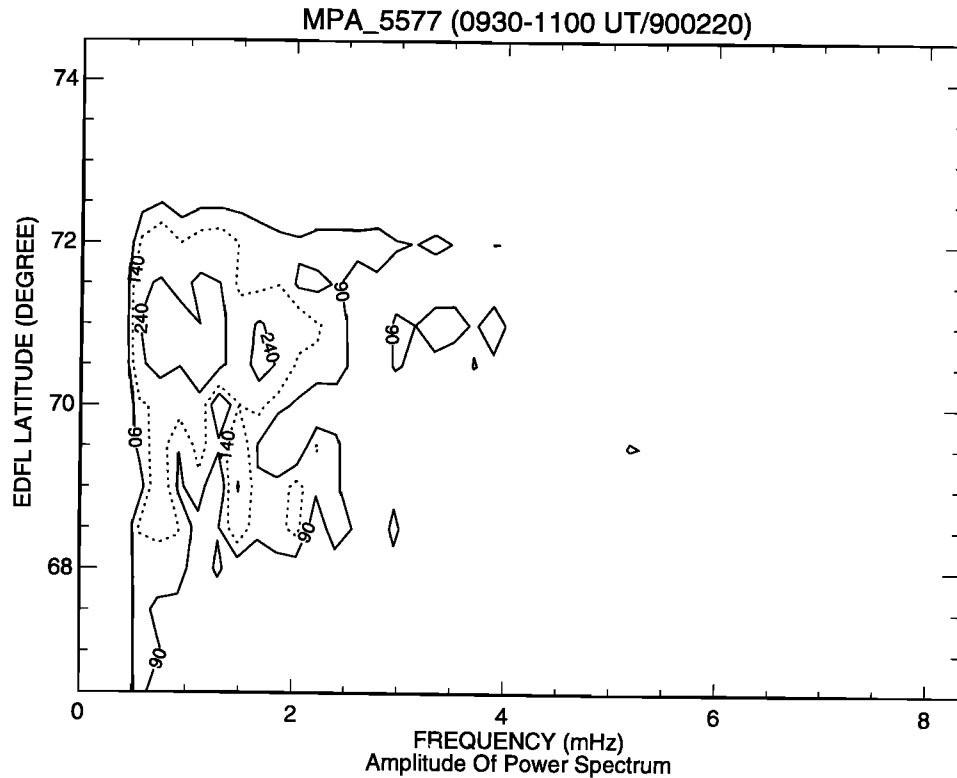


Figure 5. Contour map of auroral emission as a function of latitude and frequency for the data shown in Plate 1. The most intense emissions occur between 68° and 72° and span the frequency interval 0.5 to 2.0 mHz. At 70.5° there appears a double peak structure with maxima at about 0.9 mHz and 1.7 mHz. EDFL, eccentric dipole latitudes.

time) of 557.7 nm auroral emission for a 90 min time interval. It was constructed by combining two Canadian Auroral Network for the OPEN Program Unified Study (CANOPUS) ground meridional scanning photometers together. The lower-latitude station was Gillam (53.4°, 265.4° geodetic latitude/longitude), and the higher-latitude one was Rankin Inlets (62.8°, 267.9°). The lower-latitude station had cloud cover during the interval in question, but by also investigating a station further equatorward (Pinawa) it is clear the event corresponds to a double oval pattern with the most poleward oval occurring within the Rankin Inlets field of view. The eccentric dipole latitudes (EDFL) are 63.9° and 70.4° corresponding to L values of 6.7 and 12.4. Plate 1 clearly shows enhanced electron related emission at 70° magnetic latitude (near the zenith of Rankin Inlets). Corresponding emissions at 486.1 nm show similar structure in the proton related precipitation [Liu *et al.*, 1995]. Both the proton and electron emissions are modulated at the higher latitude with frequencies of 1 to 2 mHz. Equatorward phase motion is clearly seen. These observations occur in the early morning sector (0300-0500 magnetic local time (MLT)) and represent an isolated set of long-period auroral pulsations at high latitude. In the hour prior to 0930 UT, emissions were confined to the lower-latitude region, and after 1100 UT

the higher-latitude region remained active but without strong pulsation activity. Just prior to 0930 UT, there was some evidence of rapid poleward expansion of the auroral emissions, indicating that the higher latitude region was the formation of the poleward portion of a double oval configuration toward the end of a substorm expansion. Similar activity was described by *Elphinstone et al.* [1995b] and was attributed to the activation of the PSBL in response to the ejection of a plasmoid downtail at the start of substorm recovery. The proton emissions can then be interpreted as the auroral counterpart to the velocity dispersed ion signature (VDIS) associated with the PSBL. See *Elphinstone et al.* [1995a, 1996] for further details regarding the mapping to the magnetosphere and the relationship of this double oval to the substorm process.

Figure 5 shows a contour map of power as a function of EDFL latitude and frequency constructed from the temporal Fourier transform of the event shown in Plate 1. A filter removed low frequencies below 0.5 mHz. Evidence for strong power at frequencies below 2 mHz can be seen with the strongest power near 71° EDFL. There is evidence for two spectral peaks at 0.9 and 1.7 mHz, although the frequency resolution is not good (about 0.2 mHz). The analysis presented by *Liu et al.* [1995] also found these two frequencies in both the 557.7 and

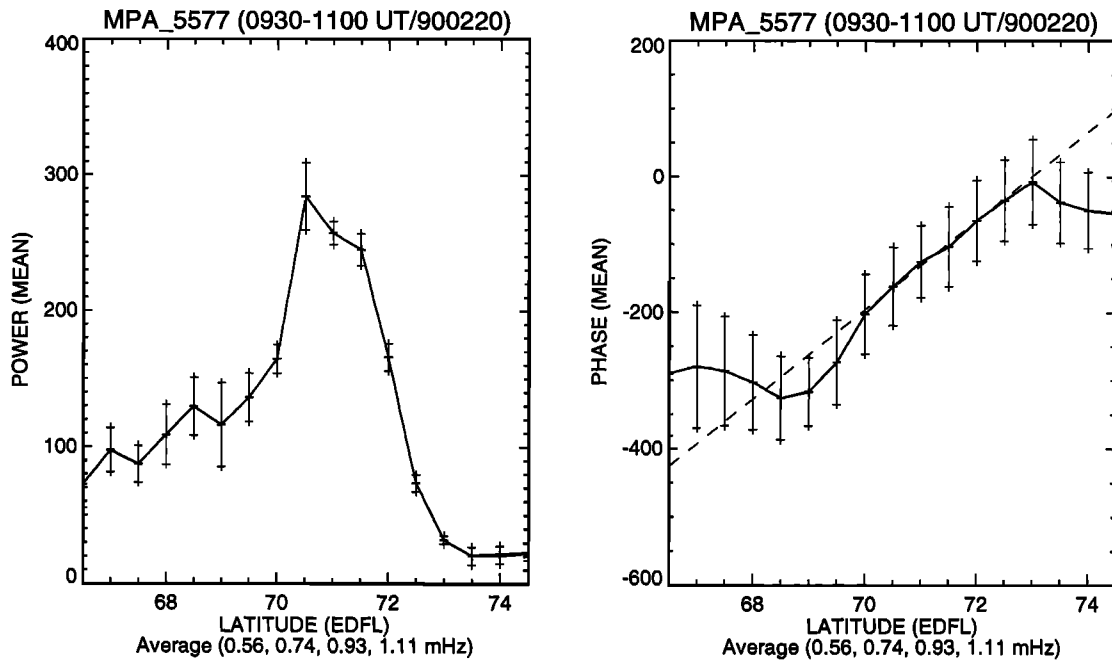


Figure 6a. The power and phase of the FFT of the data in Plate 1, averaged across the 0.9 mHz peak. Note the clear increase in phase with latitude which corresponds to equatorward phase motion. The dashed line is a least squares fit to the phase values between 70° and 72°.

486.1 nm emissions, lending support to their separate identity. We shall treat them as distinct in the following analysis.

The relationship between phase and amplitude as a function of latitude is calculated by averaging the phase and amplitude of the variation over the dominant frequency bins for each latitude. These are plotted in Fig-

ures 6a and 6b as a function of latitude for the 0.9 and 1.7 mHz peaks, respectively. There are clear progressions of phase from high latitude to low latitude across the peaks in amplitude. The total phase change is about 360°. Note that this phase change confirms the equatorward phase motion seen by eye in Plate 1. It is much greater than the 180° phase change expected for lower-

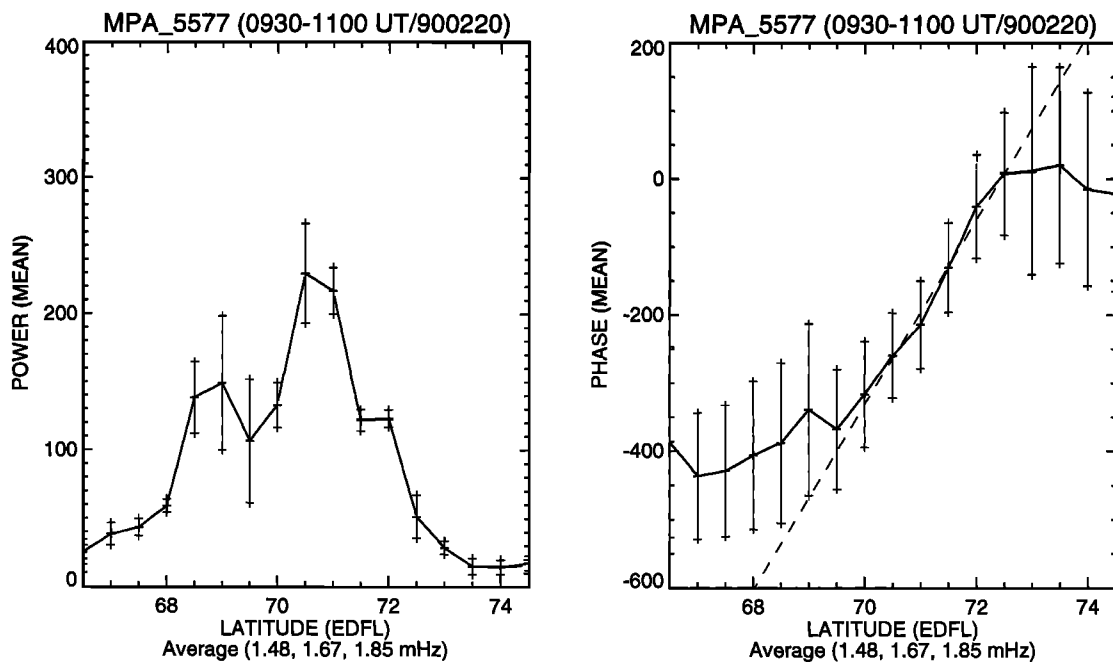


Figure 6b. Same as Figure 6a, except averaged across the 1.7 mHz peak.

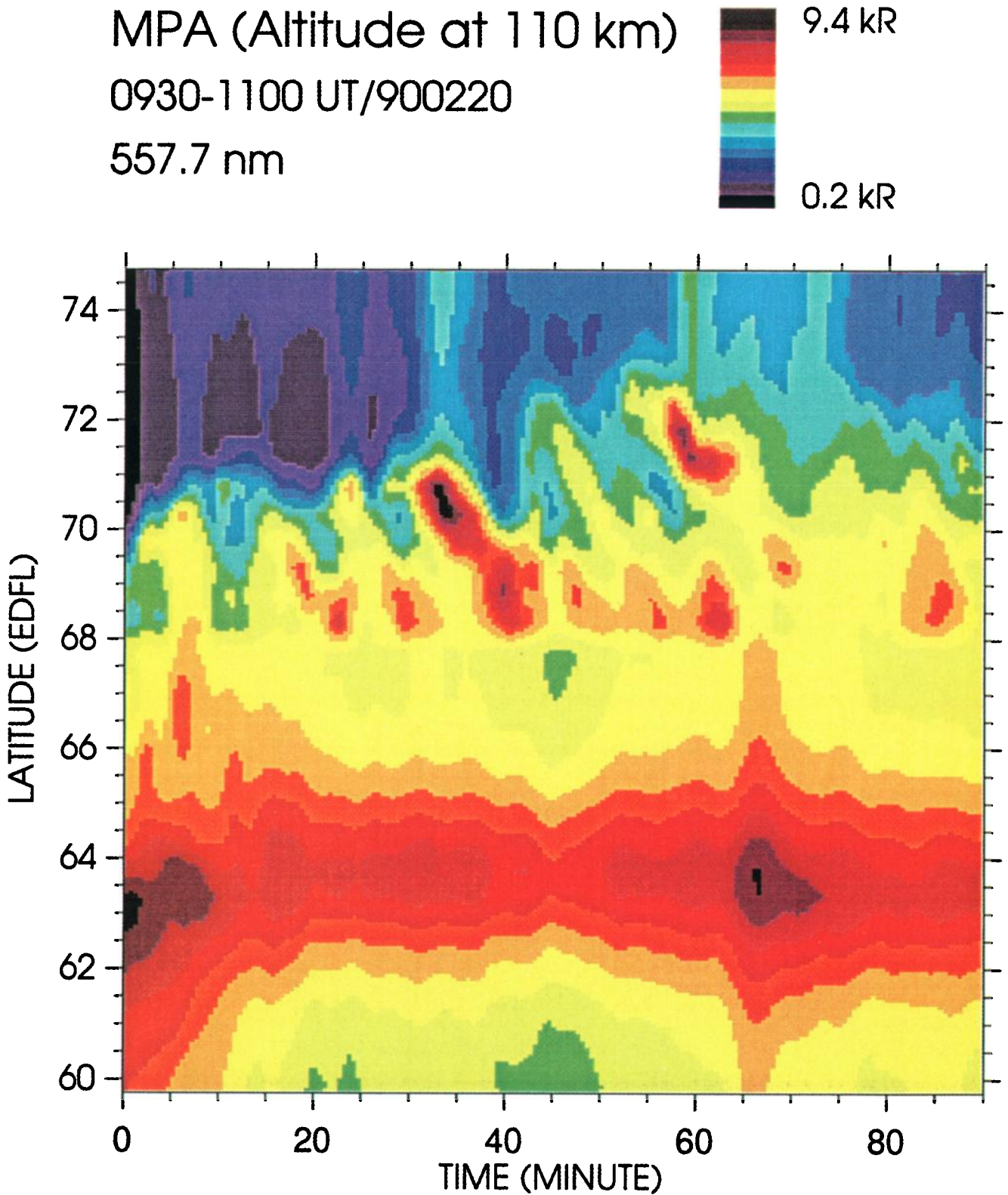


Plate 1. February 20, 1990: 557.7 nm auroral luminosity variation with latitude and time. The data is from two CANOPUS auroral scanning photometers located at Rankin and Gillam. The most poleward aurorae (between 68° and 72°) show several arcs with a period of about 8 min and a clear equatorward phase motion. The equatorward station has cloud cover.

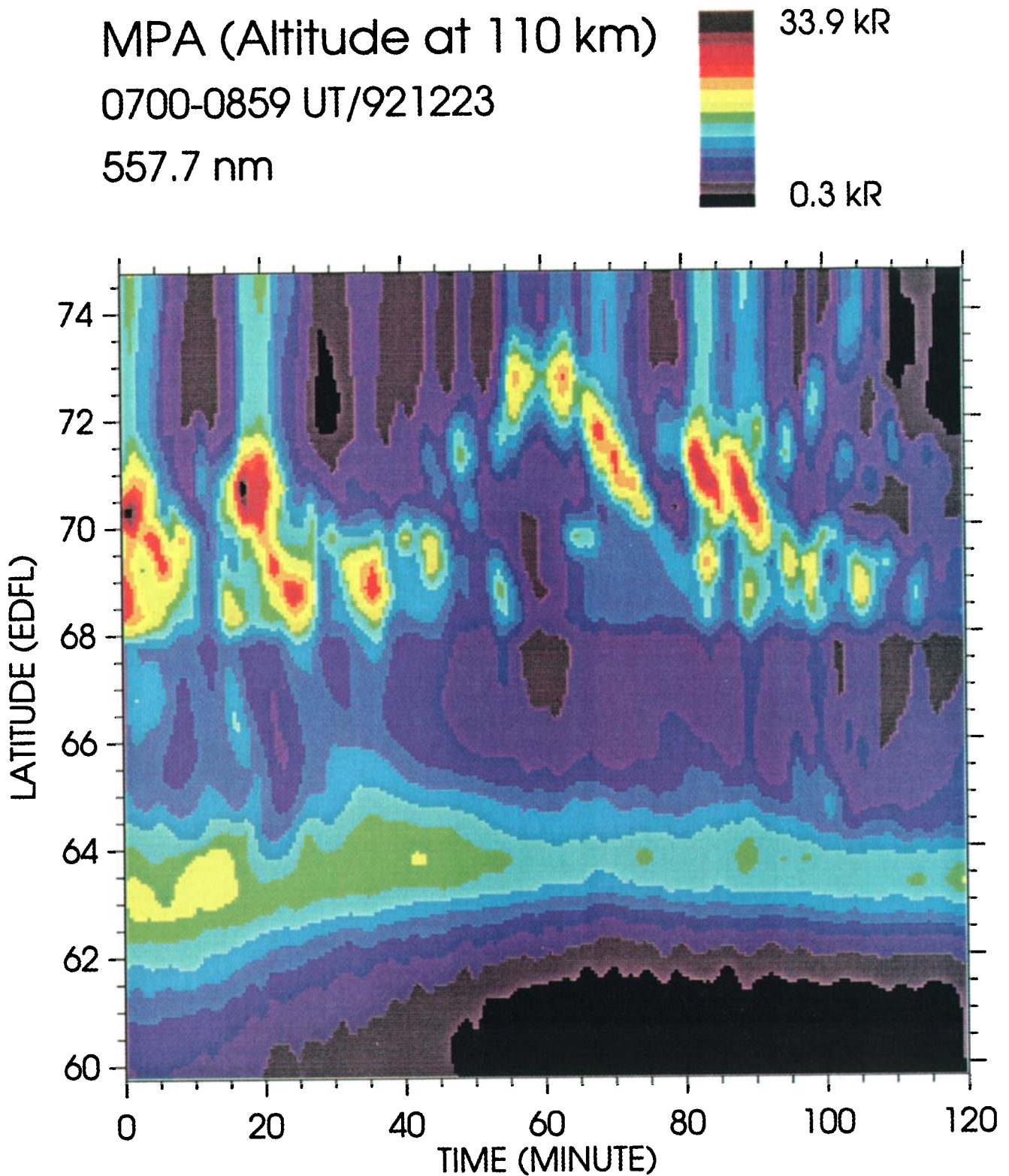


Plate 2. December 23, 1992: 557.7 nm auroral luminosity variation with latitude and time. The format is the same as in Plate 1. Again, the equatorward station has cloud cover, but the poleward station sees a clear equatorward arc motion. The first set of arcs fades about 50 min into the interval shown. A second set of auroral arcs appears after 60 min and persists for another 50 min.

latitude field line resonances which are limited by ionospheric dissipation. Least squares fits to the regions of strong power (between 70° and 72°) are shown in Figures 6a and 6b by dashed lines.

The magnitude of the equatorward phase velocity may be estimated using

$$\left| \frac{\partial \lambda}{\partial t} \right|_\phi = \left| \frac{\partial \lambda}{\partial \phi} \right|_t \cdot \left| \frac{\partial \phi}{\partial t} \right|_\lambda \quad (26)$$

where λ is the magnetic latitude. From the slope of the phase plot in Figure 6a we find $|\partial \lambda / \partial \phi|_t = 0.015 \pm 0.006$ degrees of latitude per degree of phase. The quantity $|\partial \phi / \partial t|_\lambda$ is simply ω_A . Taking the effective Alfvén frequency to be the median frequency of 0.84 mHz, $|\partial \phi / \partial t|_\lambda$ in units of degrees s^{-1} is $360 \times 0.84 \times 10^{-3}$, and we find $|\partial \lambda / \partial t|_\phi = (4.6 \pm 1.5) \times 10^{-3}$ degrees s^{-1} , which is equivalent to 0.51 ± 0.15 km s^{-1} in the ionosphere. A similar analysis for Figure 6b yields $|\partial \lambda / \partial \phi|_t = 0.0073 \pm 0.002$ degrees of latitude per degree of phase. The median frequency is 1.67 mHz, so $|\partial \phi / \partial t|_\lambda$ in units of degrees s^{-1} is $360 \times 1.67 \times 10^{-3}$, giving $|\partial \lambda / \partial t|_\phi \approx (4.4 \pm 1.5) \times 10^{-3}$ degrees s^{-1} , or 0.50 ± 0.15 km s^{-1} in the ionosphere. The phase speeds of the two oscillations differ by less than the accuracy of measurements, suggesting that the phase velocity is independent of frequency. That is, higher frequencies imply smaller phase slopes such that the product is constant. These notions are also supported by the fact that

there appears to be a fairly constant slope in the RTI plot (Plate 1) independent of the repetition period of the brightenings.

4.2. December 23, 1992, Event

A second set of 557.7 nm emission is shown in Plate 2 again from the meridian scanning photometers at Gillam and Rankin Inlets. The lower station ($< 68^\circ$ latitude) has intermittent cloud cover (being clear between 0730-0800 and 0815-0900 UT), but equatorward moving arcs are clearly present at the upper station. The magnetic local time of the observations spans 0100-0300 hours, and the field lines from latitudes around 70° are expected to map to the PSBL. The equatorward moving arcs appear to fall into two groups (the second group starting about 55 min into the observing period), perhaps as a result of two releases of energy from the distant plasma sheet. Figure 7 shows the power of the signal as a function of frequency and latitude for the second set of arcs. There are clear, well-separated peaks at 1.0 and 3.1 mHz. We note that the spectrum of the first set of arcs contains peaks at exactly the same frequencies (not shown), but because the phases of the two groups are unrelated, we shall focus solely on the second group.

The latitudinal variation of the average amplitude and phase for the two peaks is shown in Figures 8a and 8b. The 1 mHz peak data (Figure 8a) has a gradient of

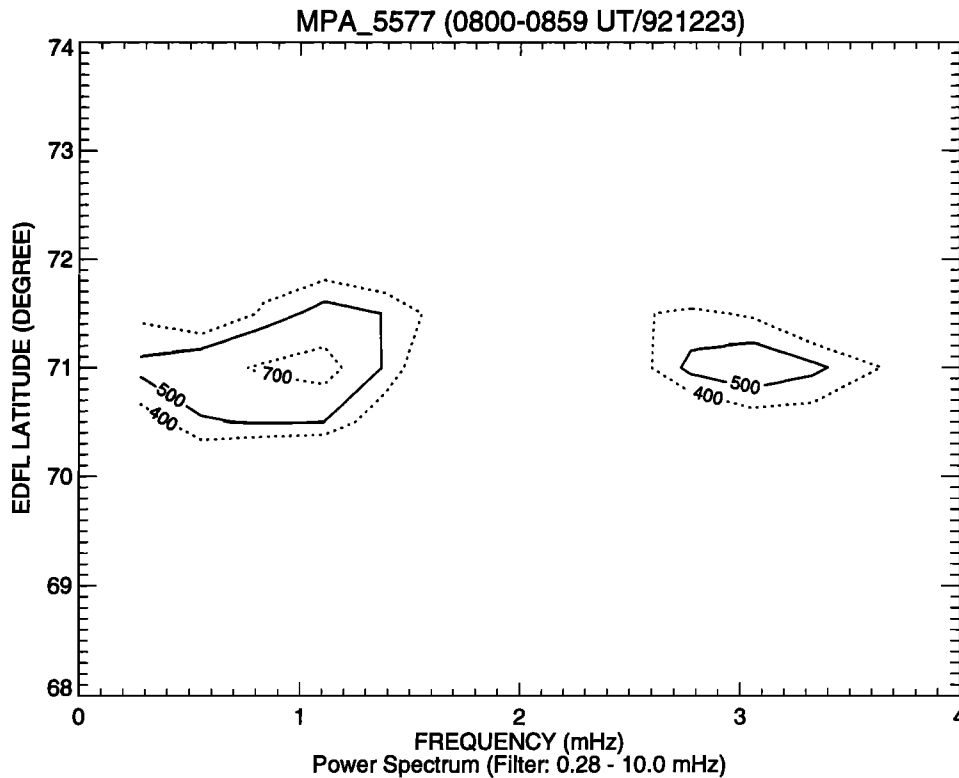


Figure 7. Contour map of auroral emission as a function of latitude and frequency for the data shown in Plate 2. At a latitude of 71° , there are two well-separated spectral peaks at 1.0 and 3.1 mHz.

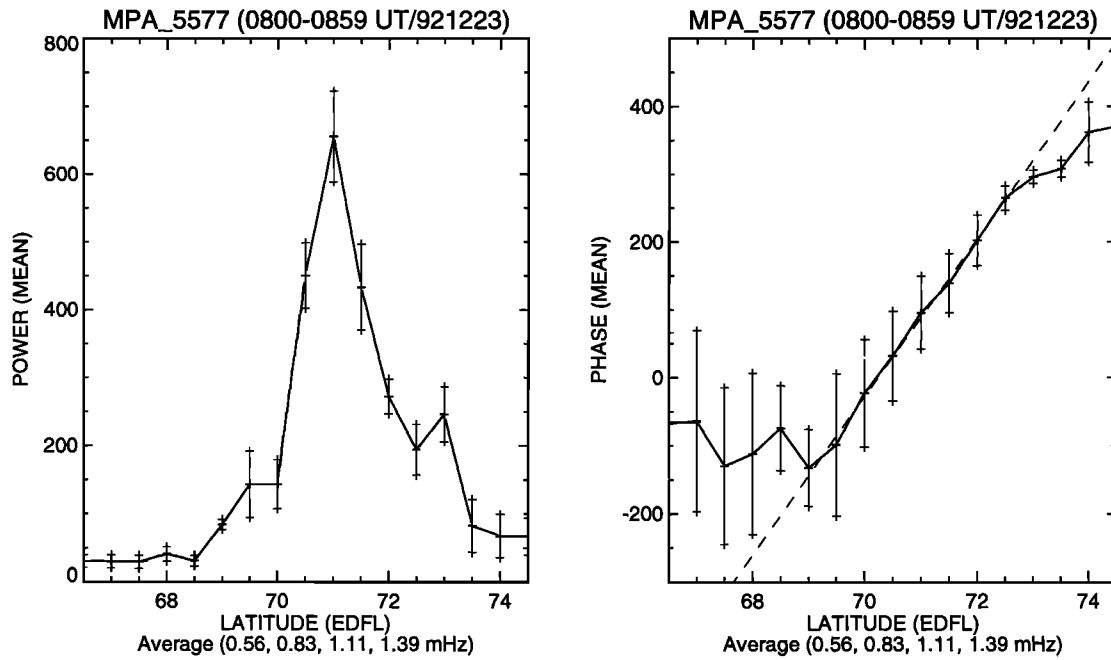


Figure 8a. The power and phase of the FFT of the data in Plate 2, averaged across the 1.0 mHz peak. Note the clear increase in phase with latitude which corresponds to equatorward phase motion. The dashed line is a least squares fit to the phase values between 70.5° and 72°.

116 ± 20 degrees of phase per degree of latitude and a median frequency of 0.97 mHz, yielding a phase speed of $0.0030 \pm 0.0005 \text{ deg s}^{-1}$ or $0.34 \pm 0.06 \text{ km s}^{-1}$. The 3.1 mHz peak data bins have a phase gradient of $164 \pm 39 \text{ deg/deg}$ across the peak and a median frequency of 3.06 mHz, giving a phase speed of $0.0068 \pm 0.0015 \text{ deg s}^{-1}$ or $0.76 \pm 0.18 \text{ km s}^{-1}$. The phase speeds of these two signals are clearly different, unlike the previous data example.

5. Theory and Observations

When coordinated data sets of ionospheric observations and satellite data from the tail exist, there is considerable scope for checking the consistency of theory and data, and thereby deepening our understanding of the tail and its coupling to the ionosphere. For example, the timing of observations of waves in the tail and ionosphere provides important information. Indeed, the

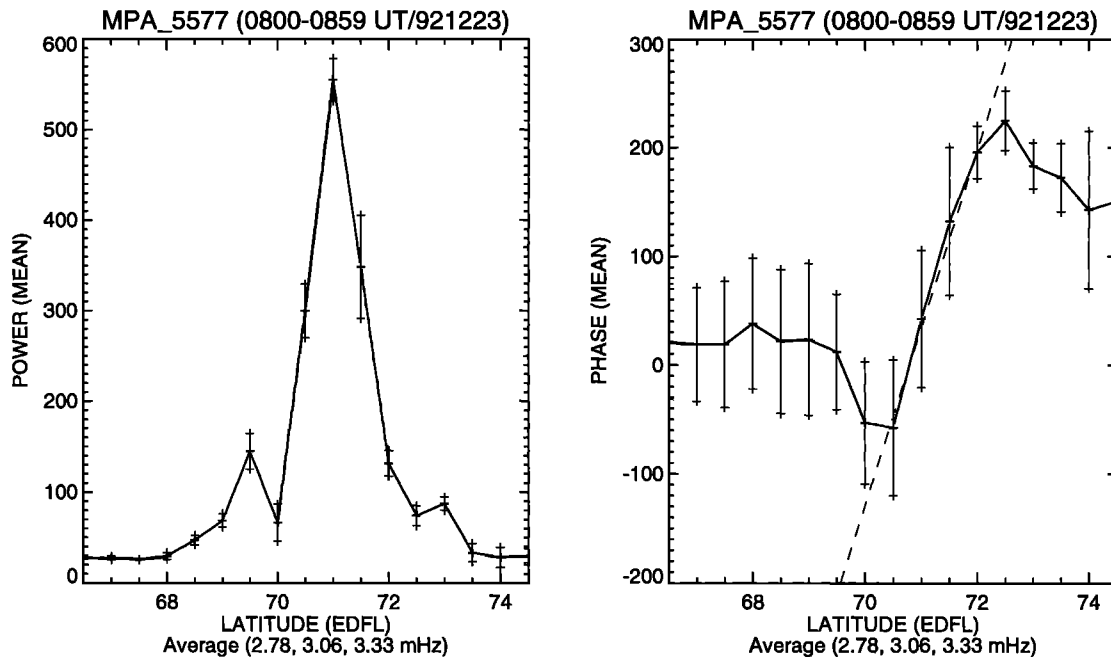


Figure 8b. Same as Figure 8a, except averaged across the 3.1 mHz peak.

simple observation of waves by a satellite can place a useful constraint upon where the waves were generated. If the equilibrium of the tail waveguide is known (e.g., $V_A(z)$) this will permit the accurate construction of a dispersion diagram for the system from which the coupling sites and group velocities may be predicted.

It is generally accepted that magnetometer and radar data are measuring the magnetic and velocity fields of magnetospheric ULF waves. Consequently, the phase motion of these data can be directly related to the phase velocity of the magnetospheric MHD waves. When dealing with optical auroral emissions, we need to be more careful, since these emissions reflect the details of the particle acceleration process as well as the magnetospheric waves which are known to modulate them. For example, it is interesting to note that the ratio of the frequencies of the two power peaks in Figure 5 (0.9 and 1.7 mHz) is very close to 2, while the corresponding ratio for Figure 7 is very close to 3. Frequency doubling is a classic signature of a nonlinear coupling process, which may be operating in the first data set. Of course, it is also possible that each spectral peak is associated with a single waveguide/Alfvén harmonic. Successive harmonics are often related by approximately integer frequency ratios in appropriate limits. There is also direct evidence from *Xu et al.* [1993] that the frequencies of optical emissions and ULF waves are the same. Given that Alfvén waves with the structure given in equation (15) have the same spatial scales of field, flow, and field-aligned current, the simplest assumption we can make is that the optical emission associated with the field-aligned current also has the same scale. We shall adopt the simplest model here and assume that the phase velocity of the optical emission can be identified with the phase velocity of MHD waves in the magnetosphere. In this scenario the separate spectral peaks in Figures 5 and 7 are produced by different tail waveguide harmonics.

5.1. February 20, 1990, Event

We do not attempt a detailed comparison here, but we show that the data in Plate 1 are consistent with typical tail parameters and a source of waves about 30 R_E downtail. To begin, we need to convert the latitudinal phase speed of section 4 to a phase speed in z to allow comparison with the model. This requires us to estimate the mapping of field lines from the ionosphere into the tail. The exact details will depend upon the model and the Kp index. We employed the Tsyganenko 1987 and 1989 models, both with $Kp = 2$ and 5. All model permutations were used to map field lines with a 1° latitudinal separation at 71° and magnetic local time of 2.4 to different distances down tail. The field line separation (in z) at a given distance could vary by up to 50% depending upon the model. We found the following average separations (α): $\alpha = 0.55, 0.9, 1.2,$ and $1.6 R_E/\text{degree}$ at 10, 20, 30, and 40 R_E downtail, respectively. Using this mapping function, it is possible

to convert the phase speed in the ionosphere observed in Plate 1 (mean for both peaks being $0.0045 \text{ deg s}^{-1}$) into a phase speed in the tail where the leading edge Alfvén waves were excited.

We do not construct a realistic dispersion diagram for the present study but simply take typical values for the Alfvén speed in the lobe of $V_A(\text{LO}) = 600 \text{ km s}^{-1}$, and in the plasma sheet of $V_A(\text{PS}) = 150 \text{ km s}^{-1}$. The ratio $\delta = V_A(\text{PS})/V_A(\text{LO})$ should be small, and is 0.25 for the above values. The Alfvén speed in the PSBL where the Alfvén waves are excited will lie between $V_A(\text{PS})$ and $V_A(\text{LO})$. For the present estimates we assume $V_A(\text{PSBL}) \approx \frac{1}{2}(V_A(\text{PS}) + V_A(\text{LO})) \equiv \frac{1}{2}V_A(\text{LO})(1 + \delta)$. We also need to evaluate the Alfvén speed gradient in the PSBL. Assuming the change occurs over a length l_z , we have $|dV_A/dz|_{\text{PSBL}} \approx (V_A(\text{LO}) - V_A(\text{PS}))/l_z \equiv (1 - \delta)V_A(\text{LO})/l_z$. If the source of waves is a distance x_0 downtail, they will be observed in the ionosphere a time t_0 after excitation. Inverting (20) gives

$$t_0 = \frac{V_A(\text{PSBL})}{|V_{pz}| |dV_A/dz|} \approx \frac{l_z}{2|V_{pz}|} (1 + 2\delta) \quad (27)$$

and

$$x_0 = V_A(\text{PSBL})t_0 \approx l_z(1 + 3\delta) \frac{V_A(\text{LO})}{4|V_{pz}|} \quad (28)$$

Equation (28) may be employed to estimate the value of l_z that is consistent with a source of waves excited a distance x_0 downtail, given the observed phase speed of $0.0045 \text{ deg s}^{-1}$ and mapping function $\alpha(x_0)$. For sources located at 10, 20, 30, and 40 R_E downtail, we find $l_z = 0.6, 2.0, 4.0,$ and $7.2 R_E$, respectively. A typical PSBL thickness is 3 or 4 R_E , suggesting the source was 25 or 30 R_E downtail. Equation (27) implies these waves are seen in the ionosphere 8 or 9 min after excitation. The ionospheric observations of waves may continue up to a time $t_f = x_0/V_{g\parallel}$. The actual period of observation (Δt) must satisfy the relation $\Delta t \leq x_0/V_{g\parallel} - x_0/V_A(\text{PSBL})$, which may be rearranged to give

$$V_{g\parallel} \leq \frac{1}{\Delta t/x_0 + 1/V_A(\text{PSBL})} \quad (29)$$

Since the aurorae were observed for ~ 1 hour, these numbers suggest $V_{g\parallel}(\text{PSBL}) \leq 40 \text{ km s}^{-1}$. Indeed, the analysis leading to (25) and the fact that the slope of the arcs changes little during the observation period indicate that $V_{g\parallel} \ll 40 \text{ km s}^{-1}$, suggesting that we are observing Alfvén waves produced by fairly small k_{\parallel} (i.e., large parallel wavelength) fast mode components. We can check this by estimating $k_{\parallel A} = \omega_A/V_A(\text{PSBL})$, which yields field-aligned wavelengths of 65 and 35 R_E for the 0.9 and 1.7 mHz peaks. These wavelengths are indeed much larger than the 3 or 4 R_E scale of the PSBL (l_z) and suggest that we have a consistent, if approximate, view of the events that could produce the observations in Plate 1. Simultaneous ground magnetometer

and optical observations combined with tail lobe magnetic field observations further support this view of a coupling between the poleward portion of the double oval (PSBL) and a perturbed magnetotail excited by a plasmoid leaving the magnetotail at the beginning of substorm recovery [Elphinstone *et al.*, 1995a]. When further auroral observations are complemented by suitable satellite observations of the tail, it should be possible to get a more comprehensive description of the equilibrium and waves.

5.2. December 23, 1992, Event

It is interesting to note that our unapproximated equation (24) for the phase speed of the waves at x_0 shows that this speed may increase in time. This is the opposite behavior to phase mixing on closed field lines or single k_{\parallel} mode models which have the phase speed decrease in time [e.g., Liu *et al.*, 1995, Figure 6]. As noted above, the ordering of quantities may mean that the phase speed appears to be fairly constant. If waves are observed in the ionosphere for a significant fraction of t_f , it should be realized that the Alfvén waves observed at later times are not being excited at the original source region (a distance x_0 downtail) but at a distance $x'_0 = x_0 - V_{g\parallel}(z)t'$. It is the quantity x'_0 that should be used in the calculation of the phase properties of the waves observed in the ionosphere at t' , and the fact that α and possibly l_z will vary for these portions of the waves should be allowed for. These are fairly subtle points, and we need to decide what (if any) is the observed systematic variation of V_{pz} with time before concerning ourselves with them. Indeed, if only three or four cycles are ever observed, it may be hard to determine the phase speed variation from cycle to cycle accurately enough to illustrate these issues.

Leaving aside the issue of ionospheric phase speed variation with time, it is evident from our analysis of the second data set (December 23, 1992) that the two spectral peaks have different phase speeds by a factor of about 2. Since we calculate the phase speed by observing several arcs persisting for about 50 min (for the data in Figures 7 and 8), we are really calculating the average phase speed during the wave's lifetime. Employing the unapproximated expression for the phase speed (24) and estimating V_A and its gradient in the PSBL as before, we find

$$|V_{pz}(x_0, \text{PSBL}, t')| = \frac{(1 + 3\delta)l_z V_A(\text{LO})}{4x_0} \times \left[1 - \frac{t'/x_0}{1/V_{g\parallel} - 2(1 - \delta)/V_A(\text{LO})} \right]^{-1} \quad (30)$$

The second set of arcs persist for about 50 min, during which time the phase speed of the arcs may change. Our "average" phase speed for this interval can be thought of as representing the phase speed of the arcs about 25 min into this interval. Adopting $t' = 25$ min, we can use (30) to infer l_z for different source locations downtail

given the average phase speed and field line mapping function $\alpha(x_0)$. Since the present analysis requires some knowledge of $V_{g\parallel}$, we shall start with the 1 mHz peak and assume that it is similar to the 0.9 mHz peak of the first event (February 20, 1990). Section 5.1 concluded that $V_{g\parallel}$ for this mode was much less than 40 km s^{-1} , so we shall simply assume $V_{g\parallel} = 15 \text{ km s}^{-1}$. Calculating the implied PSBL width (l_z) for $x_0 = 10, 20, 30,$ and $40 R_E$ yields $l_z = 0.3, 1.1, 2.5,$ and $4.5 R_E$, respectively. A typical PSBL width of 3 or 4 R_E places the source location at about 35 R_E downtail, and the waves would take about 10 min to reach the ionosphere.

Assuming the second spectral peak at 3.1 mHz is initiated from the same location as the 1 mHz signal, we can use the observed (average) phase speed of the 3.1 mHz peak to estimate $V_{g\parallel}$ for the second driving waveguide mode by employing (30) and setting $t' = 25$ min, $l_z = 3.5 R_E$, and $x_0 = 35 R_E$. This calculation gives $V_{g\parallel} = 70 \text{ km s}^{-1}$ for the 3.1 mHz waveguide mode. Interestingly, the fast mode time of flight is then $t_f = 53$ min for these parameters, after which time Alfvén waves should stop reaching the ionosphere. This is very close to the duration of the arc features and may account for their cessation after about 50 min. Of course, this mechanism can not be used to explain why the 1 mHz arcs have a similar duration as their time of flight is about 4 hours. It may be that we have underestimated $V_{g\parallel}$ for the 1 mHz mode, but we note if the two modes have similar group velocities, equation (30) shows that they have similar phase speeds for all t' , so their average phase speeds will be similar if they survive for the same time. It may be that the 1 mHz waves do not survive for 4 hours because most of the fast mode energy has been coupled to the Alfvén waves after 50 min, or the fast mode waves have leaked out of the flanks of the tail [Liu *et al.*, 1995] to the extent that only small amplitude Alfvén waves (if any) are driven after 50 min, and they are not of sufficient amplitude to produce optical emissions.

6. Summary

The phase properties of Alfvén waves have been studied for typical magnetospheric equilibria. Alfvén waves on near-Earth closed field lines should show a poleward phase motion (as is generally observed by auroral radar), unless they are close to the plasmopause, in which case the motion may be reversed. Those Alfvén waves generated in the PSBL should show an equatorward motion. Observations of arcs from the poleward portion of the double oval (which are believed to map to the PSBL [Elphinstone *et al.*, 1995a]) are presented and show obvious equatorward motion. Other arcs in the equatorward auroral oval on the nightside or the flanks have been well documented elsewhere and show the predicted poleward phase motion associated with dipole-like closed field lines.

Observations of ionospheric phase motions provide valuable clues to the structure of the regions of the

magnetosphere where the Alfvén waves were excited (e.g., the variation of ω_A and V_A across field lines), and this may indicate whether nighttime arcs are generated in the near-Earth region or further downtail near the PSBL. The equatorward phase velocity and its change in time can also yield properties such as the ionospheric Pedersen conductivity, the group velocity of fast modes, or the location of driving sources in the tail such as reconnection events. When these concepts are combined with satellite and ground-based data, they provide a very powerful tool for examining magnetospheric equilibria and dynamic processes such as substorms.

Acknowledgments. This work was carried out while A.N.W. was supported by a UK PPARC Advanced Fellowship. W.A. acknowledges support from the New Zealand Foundation for Research, Science and Technology under contract C01627. The work done at the University of Calgary was supported by grants from the Natural Sciences and Engineering Research Council of Canada. The CANOPUS project is supported by the Canadian Space Agency. R.D.E. would like to thank Pao Qi for his help with the Canopus data. A.N.W. thanks John Samson for many helpful discussions.

Janet G. Luhmann thanks Erling Nielsen and John Samson for their assistance in evaluating this paper.

References

- Allan, W., Plasma energization by the ponderomotive force of magnetospheric standing Alfvén waves, *J. Geophys. Res.*, **98**, 11,383, 1993.
- Allan, W., and E. M. Poulter, ULF waves—Their relationship to the structure of the Earth's magnetosphere, *Rep. Prog. Phys.*, **55**, 533, 1992.
- Allan, W., and A. N. Wright, Large- m waves generated by small- m field line resonances via the nonlinear Kelvin-Helmholtz instability, *J. Geophys. Res.*, **102**, 19,927, 1997.
- Allan, W., and A. N. Wright, Hydromagnetic wave propagation and coupling in a magnetotail waveguide, *J. Geophys. Res.*, **103**, 2359, 1998.
- Brooks, D., Radio auroral echoes associated with sudden commencements and their possible use in measurement of magnetospheric ion densities, *J. Atmos. Terr. Phys.*, **29**, 589, 1967.
- Elphinstone, R. D., and D. J. Hearn, The aurora and its relation to magnetospheric processes, *Adv. Space Res.*, **13**, No. 4, 17, 1993.
- Elphinstone R. D., et al., The double oval UV auroral distribution, 1, Implications for the mapping of auroral arcs, *J. Geophys. Res.*, **100**, 12,075, 1995a.
- Elphinstone R. D., et al., The double oval UV auroral distribution: 2. The most poleward arc system and the dynamics of the magnetotail, *J. Geophys. Res.*, **100**, 12,093, 1995b.
- Elphinstone R. D., J. S. Murphree, and L. L. Cogger, What is a global auroral substorm?, *Rev. Geophys.*, **34**, 169, 1996.
- Fenrich, F. R., J. C. Samson, G. Sofko, and R. A. Greenwald, ULF high- and low- m field line resonances observed with the Super Dual Auroral Radar Network, *J. Geophys. Res.*, **100**, 21,535, 1995.
- Goertz, C. K., and R. A. Smith, The thermal catastrophe model of substorms, *J. Geophys. Res.*, **94**, 6581, 1989.
- Hood, A. W., J. Ireland, and E. R. Priest, Heating of coronal holes by phase mixing, *Astron. Astrophys.*, **318**, 957, 1997.
- Hughes, W. J., The effect of the atmosphere and ionosphere on long-period magnetospheric micropulsations, *Planet. Space Sci.*, **22**, 1157, 1974.
- Hughes, W. J., Magnetospheric ULF waves: A tutorial with a historical perspective, in *Solar Wind Sources of Magnetospheric Ultra-Low-Frequency Waves*, *Geophys. Monogr. Ser.* 81, edited by M. J. Engebretson, K. Takahashi, and M. Scholer, p.1, AGU, Washington, D.C., 1994.
- Ireland, J., and E. R. Priest, Phase mixing in dissipative Alfvén waves, *Sol. Phys.*, **173**, 31, 1997.
- Kaneda, E., S. Kokubun, T. Oguti, and T. Nagata, Auroral radar echoes associated with Pc5, *Rep. Ionos. Space Res. Jpn.*, **18**, 165, 1964.
- Keys, J. G., Pulsating auroral radar echoes and their possible hydromagnetic association, *J. Atmos. Terr. Phys.*, **27**, 385, 1965.
- Liu, W. W., B.-L. Xu, J. C. Samson, and G. Rostoker, Theory and observations of auroral substorms: A magnetohydrodynamic approach, *J. Geophys. Res.*, **100**, 79, 1995.
- Mann, I. R., A. N. Wright, and P. S. Cally, Coupling of magnetospheric cavity modes to field line resonances: A study of resonance widths, *J. Geophys. Res.*, **100**, 19,441, 1995.
- McDiarmid, D. R., and W. Allan, Simulation and analysis of auroral radar signatures generated by a magnetospheric cavity mode, *J. Geophys. Res.*, **95**, 20,911, 1990.
- Nielsen, E., and W. Allan, A double-resonance Pc 5 pulsation, *J. Geophys. Res.*, **88**, 5760, 1983.
- Nielsen, E., R. D. Elphinstone, D. J. Hearn, J. S. Murphree, and T. Potemra, Oval intensification event observed by STARE and Viking, *J. Geophys. Res.*, **98**, 6163, 1993.
- Poulter, E. M., W. Allan, J. G. Keys, and E. Nielsen, Plasmatrrough ion mass densities determined from ULF pulsation eigenperiods, *Planet. Space Sci.*, **32**, 1069, 1984.
- Rickard, G. J., and A. N. Wright, Alfvén resonance excitation and fast wave propagation in magnetospheric waveguides, *J. Geophys. Res.*, **99**, 13,455, 1994.
- Samson, J. C., J. A. Jacobs, and G. Rostoker, Latitude-dependent characteristics of long-period geomagnetic micropulsations, *J. Geophys. Res.*, **76**, 3675, 1971.
- Samson, J. C., T. J. Hughes, F. Creutzberg, D. D. Wallis, R. A. Greenwald, and J. M. Ruohoniemi, Observations of a detached, discrete arc in association with field line resonances, *J. Geophys. Res.*, **96**, 15,683, 1991.
- Samson, J. C., D. D. Wallis, T. J. Hughes, F. Creutzberg, J. M. Ruohoniemi, and R. A. Greenwald, Substorm intensifications and field line resonances in the nightside magnetosphere, *J. Geophys. Res.*, **97**, 8495, 1992.
- Samson, J. C., L. L. Cogger, and Q. Pao, Observations of field line resonances, auroral arcs and auroral vortex structures, *J. Geophys. Res.*, **101**, 17,373, 1996.
- Seboldt, W., Nonlocal analysis of low-frequency waves in the plasma sheet, *J. Geophys. Res.*, **95**, 10 471, 1990.
- Southwood, D. J., Some features of field line resonances in the magnetosphere, *Planet. Space Sci.*, **22**, 483, 1974.
- Tamao, T., Transmission and coupling resonance of hydromagnetic disturbances in the non-uniform Earth's magnetosphere, *Sci. Rep. Tohoku Univ.*, **5**, 17, 43, 1965.
- Walker, A. D. M., R. A. Greenwald, W. F. Stuart, and C. A. Green, STARE auroral radar observations of Pc5 geomagnetic pulsations, *J. Geophys. Res.*, **84**, 3373, 1979.
- Wei, C. Q., J. C. Samson, R. Rankin, and P. Frycz, Electron inertial effects on geomagnetic field line resonances, *J. Geophys. Res.*, **99**, 11,265, 1994.
- Wright, A. N., MHD theory of magnetic pulsations, in *Physical Signatures of Magnetospheric Boundary Layer Pro-*

- cesses, edited by J. A. Holtet and A. Egeland, p. 329, Kluwer Acad., Norwell, Mass., 1994a.
- Wright, A. N., Dispersion and wave coupling in inhomogeneous MHD waveguides, *J. Geophys. Res.*, *99*, 159, 1994b.
- Wright, A. N., and W. Allan, Are two-fluid effects relevant to ULF pulsations?, *J. Geophys. Res.*, *101*, 24,991, 1996a.
- Wright, A. N., and W. Allan, Structure, phase motion, and heating within Alfvén resonances, *J. Geophys. Res.*, *101*, 17,399, 1996b.
- Xu, B.-L., J. C. Samson, W. W. Liu, F. Creutzberg, and T. J. Hughes, Observations of optical aurora modulated by resonant Alfvén waves, *J. Geophys. Res.*, *98*, 11,531, 1993.
- W. Allan, National Institute of Water and Atmospheric Research, P. O. Box 14-901, Kilbirnie, Wellington, New Zealand. (w.allan@niwa.cri.nz)
- L. L. Cogger and R. D. Elphinstone, Department of Physics and Astronomy, University of Calgary, Calgary, AB, Canada T2N 1N4. (cogger@phys.ucalgary.ca, rob@hobbes.phys.ucalgary.ca)
- A. N. Wright, Mathematical Institute, University of St. Andrews, St. Andrews, Fife KY16 9SS, Scotland. (andy@dcs.st-and.ac.uk)

(Received May 6, 1998; revised October 5, 1998; accepted January 6, 1999.)